JOURNAL OF MATERIALS SCIENCE **39** (2004) 5161–5167

Factors influencing the kinetics of electrochemical reactions in milling

V. VARGHESE*, K. CHATTOPADHYAY
Department of Metallurgy, Indian Institute of Science, Bangalore 560012, India
E-mail: varghese@platinum.metalrg.iisc.ernet.in

A. NARAYANASAMY
Materials Science Centre, Department of Nuclear Physics, University of Madras, Guindy Campus, Chennai 600 025, India

Input of mechanical energy at a high rate can drive a system and induce phase transformations and chemical reactions away from equilibrium. The evolution of such a change depends on both thermodynamic as well as kinetic factors. Besides the microstructural changes like attainment of nanostructure, which alters the overall free energy, the high rate of mechanical energy input also changes the kinetics by influencing the mass transport and related processes. In order to understand these factors, we have recently started a programme of looking at the influence of mechanical energy on driving simple chemical reactions in solid state. In this presentation we shall present and discuss the results of two kinds of situation that we have studied. The first one is simple electrochemical replacement reactions between metals and metal sulphates in solid state. We show that the mechanical milling alters the kinetics of these reactions, which can be rationalized by considering the phenomena taking place at the microscopic level. For example we will show that the crystal structure of the sulphate and the nature of the reaction product at the interface influence the mechanochemistry significantly. It is even possible in some special cases to alter the direction of the chemical reaction. In the second set of results we shall present the effect of mechanical milling on the site occupancy in ferrites, which can lead to a significant change in magnetic behaviour.

1. Introduction

Mechanochemical reactions gathered wide acceptability in recent times due to its potential to drive the reactions at ambient conditions which are either not possible or require vigorous conditions in conventional processing routes [1–4]. For example, while the unfavorable decomposition steps restrict the high temperature chemical reactions of a number of materials, they can be easily brought about through milling at room temperature itself. Similarly, while the solubility of materials restricts the use of solution chemistry, milling bypasses such limitations [5]. The reduced particle size of the products of milling makes it a more desirable processing route [6].

Evidently, mechanical energy input influences the chemical reactions and thus opens up new possibilities of materials synthesis through a combination of chemical reaction and mechanical energy. Understanding the processes that take place with the input of the mechanical energy at a rapid rate would help to have better control over the process. With this aim, we have made an attempt to understand the process by analyzing the behavior of simple electrochemical systems under milling. Parallel experiments in solution route were designed to compare and contrast and thereby unambiguously highlight the significant factors that influence the mechanochemical changes.

2. The role of thermodynamics

The cementation reaction where iron displaces copper from copper sulphate is well known in solution chemistry. A large driving force exists for this electrochemical displacement of copper in solid state too. We have seen that iron can displace copper, also from copper sulphate pentahydrate crystals through a double decomposition if they are milled together [7].

Expecting a faster displacement of copper due to steeper driving force, an equimolar mixture of $CuSO_4 \cdot 5H_2O$ and Mn was also subjected to milling. The milling parameters and experimental conditions are given in Table I. Though the reaction was faster, the products were different from that in a double decomposition. In spite of steeper driving force for the

*Author to whom all correspondence should be addressed.

TABLE I List of milling experiments and the milling conditions

System	Mill	r.p.m	Material of vial & balls	Ball-to-powder mass ratio	Medium
Mn-$CuSO_4{\cdot}5H_2O$	P-7	525	WC	8:1	Toluene
Co-$CuSO_4{\cdot}5H_2O$	P-7	525	WC	8:1	Toluene
Pb-$CuSO_4{\cdot}5H_2O$	P-7	525	WC	8:1	Toluene

double electron transfer in copper displacement, the single electron reduction to cuprous oxide along with hydrogen evolution was the most important change noticed. The hydrogen evolution from the sample in initial period of milling was visually found to proceed even when the milling is stopped for several hours. However, a loose physical mixture of Mn and $CuSO_4{\cdot}5H_2O$ did not have any reaction. We conclude that milling has triggered a combustion reaction in Mn-$CuSO_4{\cdot}5H_2O$ system. The reduced grain size and increased surface area have prompted the triggering of the combustion reaction. The analysis of the X-ray diffraction patterns reveals that an intermediate structure may have formed in the early stages. The d-spacings of the intermediate structure were close to that of $MnSO_4{\cdot}6H_2O$. As the milling progressed, the intensities of $CuSO_4{\cdot}5H_2O$ and Mn peaks quickly decreased while that of $MnSO_4{\cdot}4H_2O$ and Cu_2O peaks became intense (Fig. 1). The most intense reflection of $CuSO_4{\cdot}5H_2O$ disappeared within 3.5 h of milling though the pressure development inside the bowl continued for a little longer. Further milling up to 30 h did not give any significant change in the X-ray patterns. The results suggests the reaction as follows,

$$\mathrm{Mn(s) + CuSO_4{\cdot}5H_2O(s)} \rightarrow \mathrm{I(s) + H_2(g) + Cu_2O(s)} \quad (1)$$

$$\rightarrow \mathrm{MnSO_4{\cdot}4H_2O(s) + H_2(g) + Cu_2O(s)} \quad (2)$$

To compare this result with the electrochemical reactions in solution, Mn was added to 100 ml copper sulphate solution in molar proportion. On stirring with copper sulphate solution, gas evolution was noticed and it was characterized by flame test as hydrogen. The precipitate contained both copper and cuprous oxide (Fig. 2). Clearly, both double electron and single electron transfer occurred in the solution route resulting copper and, Cu_2O and hydrogen. The electrochemical calculations described below can explain the feasibility of reduction to Cu^{+1} along with hydrogen evolution.

$$\text{Half cell:} \quad \mathrm{Mn^{+2} + 2e^- \rightarrow Mn} \quad {}_1E^{\ominus} = -1.03\ \mathrm{V} \quad (3)$$

Copper sulphate being a salt of weak base and strong acid, the solution would contain the weakly dissociated $Cu(OH)_2$, which can also take part in reaction

$$\mathrm{Cu(OH)_2 + 2e^- \rightarrow Cu + 2OH^-} \quad {}_2E^{\ominus} = -0.224\ \mathrm{V} \quad (4)$$

$$\mathrm{Cu^+ + 1e^- \rightarrow Cu} \quad {}_3E^{\ominus} = 0.522\ \mathrm{V} \quad (5)$$

$$\mathrm{2H_2O + 2e^- \rightarrow 2OH^- + H_2} \quad {}_4E^{\ominus} = -0.828\ \mathrm{V} \quad (6)$$

$2 *$ Equation $4 - 2 *$ Equation $5 +$ Equation 6 would result the half cell as follows,

$$\text{Half cell:} \quad \mathrm{2Cu(OH)_2 + 4e^- + 2H_2O \rightarrow 2Cu^+ + H_2 + 6OH^-} \quad \Delta G^{\ominus} = 3.5954\mathrm{F} \quad (7)$$

$${}_5E^{\ominus} = -\Delta G^{\ominus}/4\mathrm{F} = -0.899\ \mathrm{V}$$

$$\text{Net cell:} \quad \mathrm{2Cu(OH)_2 + 2Mn + 2H_2O \rightarrow 2Cu^+ + H_2 + 6OH^- + 2Mn^{+2}} \quad {}_RE^{\ominus} = 0.131\ \mathrm{V} \quad (8)$$

$$\rightarrow \mathrm{Cu_2O + H_2 + H_2O + 4OH^- + 2Mn^{+2}} \quad (9)$$

Since copper sulphate is in a highly hydrated form, a similar thermodynamic argument can explain the presence of Cu_2O and evolution of hydrogen in the solid state while milling $CuSO_4{\cdot}5H_2O$-Mn system. The transmission electron microscopic studies on 30 h milled and washed sample showed particles with two distinctly different morphologies, both belonging to the same phase, Cu_2O. While one type of Cu_2O particles might have formed through direct reaction

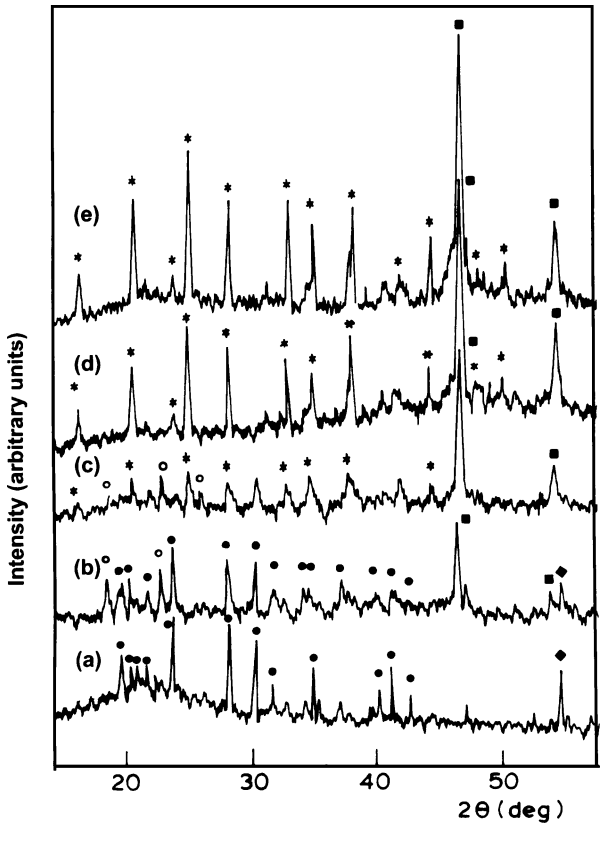

Figure 1 X-ray diffraction patterns of mechanically milled $CuSO_4{\cdot}5H_2O$-Mn system. (a) 5 min, (b) 1 h, (c) 3.5 h, (d) 5 h and (e) 30 h. ● $CuSO_4{\cdot}5H_2O$, ♦ Mn, ○ Intermediate, ∗ $MnSO_4{\cdot}4H_2O$, ■ Cu_2O.

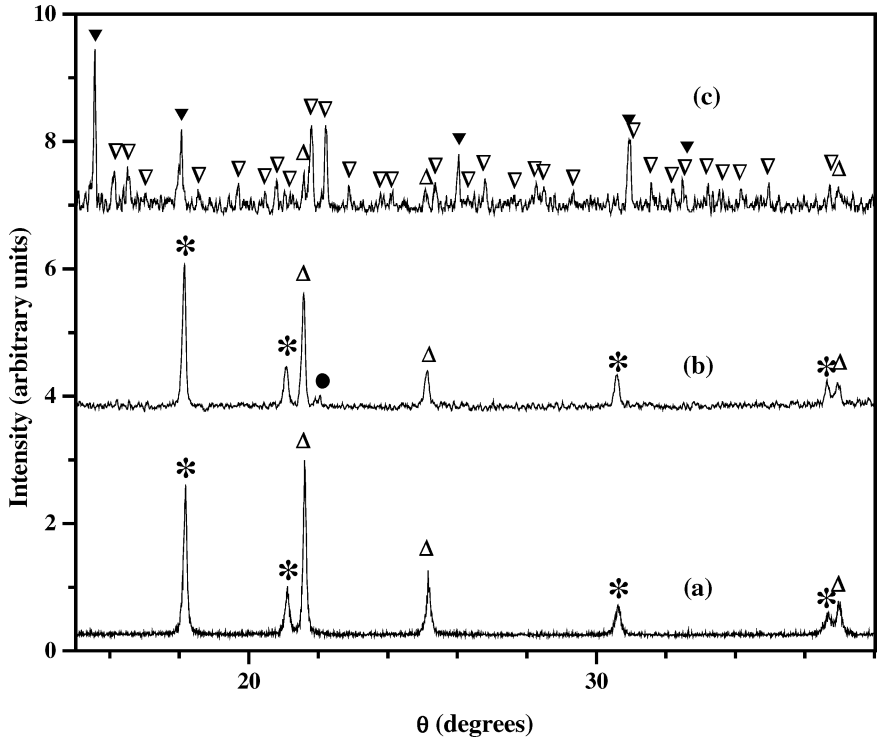

Figure 2 The X-ray diffraction patterns of the solid products obtained in (a) Mn-copper sulphate solution after 3 h, (b) Co-copper sulphate solution after 14 h and (c) Pb-copper sulphate solution after 25 h. ∗ Cu_2O, Δ Cu, ● Co, ▼ Pb and ∇ $PbSO_4$.

(Equation 9), the other might be the oxidized copper. The similarity of solid state reactions with solution route in highly hydrated systems is consistent in $CuSO_4{\cdot}5H_2O$-Co system also. There was no gas evolution on mixing Co with copper sulphate solution. The electrochemical calculations prove that there is no driving force ($_RE^{\ominus} = -0.619$ V) for the hydrogen evolution reaction by Co in solution under standard conditions. However, Cu_2O can arise from the oxidation of precipitated copper while staying more time in the solution (Fig. 2).

Milling of $CuSO_4{\cdot}5H_2O$-Co system also caused very similar changes. As the milling proceeds, the intensities of $CuSO_4{\cdot}5H_2O$ and Co peaks decreased while that of Cu_2O, Cu, $CoSO_4{\cdot}6H_2O$ and $CoSO_4{\cdot}4H_2O$ peaks became intense (Fig. 3). No pressure was developed inside the bowl with milling. Since there was no hydrogen evolution, the origin of Cu_2O is due to the oxidation of displaced Cu unlike in $CuSO_4{\cdot}5H_2O$-Mn system. Thus the results of mechanical milling of Co-$CuSO_4{\cdot}5H_2O$ system also suggest the similarity of solid-state reactions with solution route in highly hydrated systems.

3. The role of kinetics

Not only the direction of change, even the kinetics of the change followed the similar trend as in solution, in these systems. In the solution route, the driving force as well as the rate of displacement reaction goes down while going down in the electrochemical series. The reaction took only about 3 h with manganese while it took about 15 h with cobalt (Fig. 2). Consistently, while milling, the reaction was much faster in Mn-$CuSO_4{\cdot}5H_2O$ system than in Co-$CuSO_4{\cdot}5H_2O$ system. However, the trend is not followed in all the cases.

In the case of lead, the driving force for the displacement of copper from solution is very small and the reaction is extremely slow in solution (Fig. 2). It takes days for significant conversion. However, the reaction is extremely rapid when lead powder is milled with $CuSO_4{\cdot}5H_2O$ crystals (Fig. 4). The reaction is practically complete within 20 min of milling. The reaction can be stated as follows

$$\mathrm{Pb(s) + CuSO_4{\cdot}5H_2O(s)} \rightarrow \mathrm{PbSO_4(s) + Cu(s) + H_2O\,(toluene)} \quad (10)$$

The displacement of copper by lead is extremely slow in solution due to the presence of electric double layer at the interface between lead metal and solution where the redox reaction has to occur. Unless sufficient over potential is supplied the barrier by electric double layer can slow down the redox process in systems having poor driving force. Since a similar electric double layer is absent in solid state, the resistance due to double layer does not play a part in the kinetics while milling $CuSO_4{\cdot}5H_2O$-Pb system. Thus while the reaction is slow in solution, it is much faster in solid.

The higher diffusivity of lead compared to manganese and cobalt has helped $CuSO_4{\cdot}5H_2O$-Pb system to complete the reaction several times faster than $CuSO_4{\cdot}5H_2O$-Mn system and $CuSO_4{\cdot}5H_2O$-Co system. Also, since $PbSO_4$ has no water of crystallization, the water of crystallization of the copper sulfate will be released at the interface at the instant of reaction. This will clean the interface from the product phase

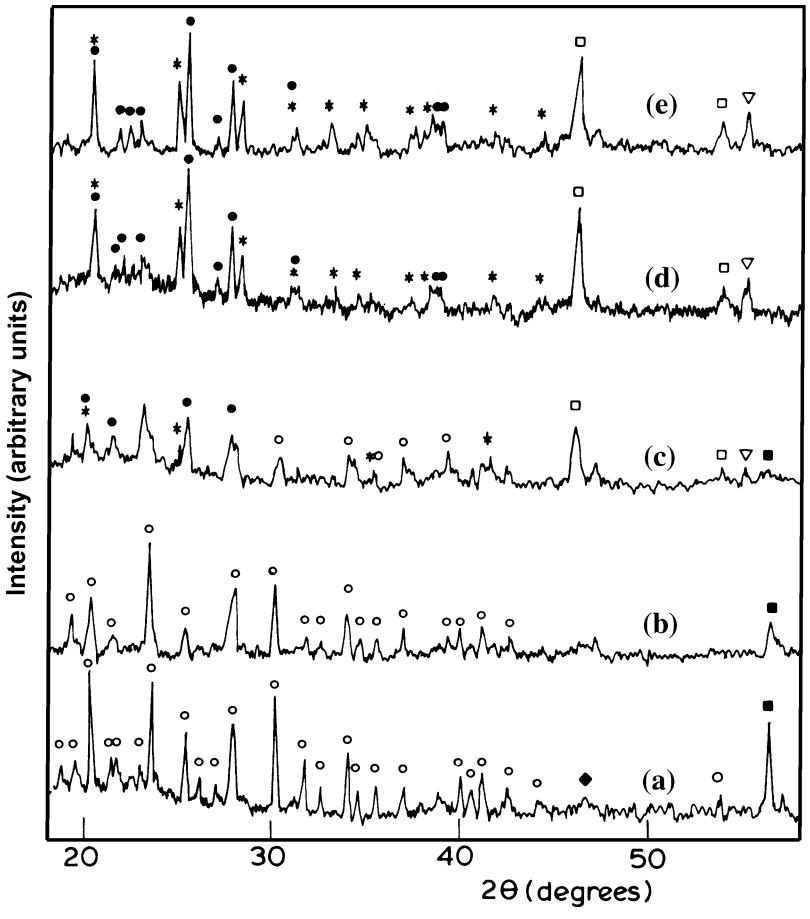

Figure 3 X-ray diffraction patterns of Co-$CuSO_4 \cdot 5H_2O$ system in P-7 with milling time. (a) 5 min, (b) 3 h (c) 12 h, (d) 30 h, and (e) 50 h. □ Cu_2O, ∇ Cu, ∗ $CoSO_4 \cdot 4H_2O$, ● $CoSO_4 \cdot 6H_2O$, ■ Co, ○ $CuSO_4 \cdot 5H_2O$ and ♦ CoO.

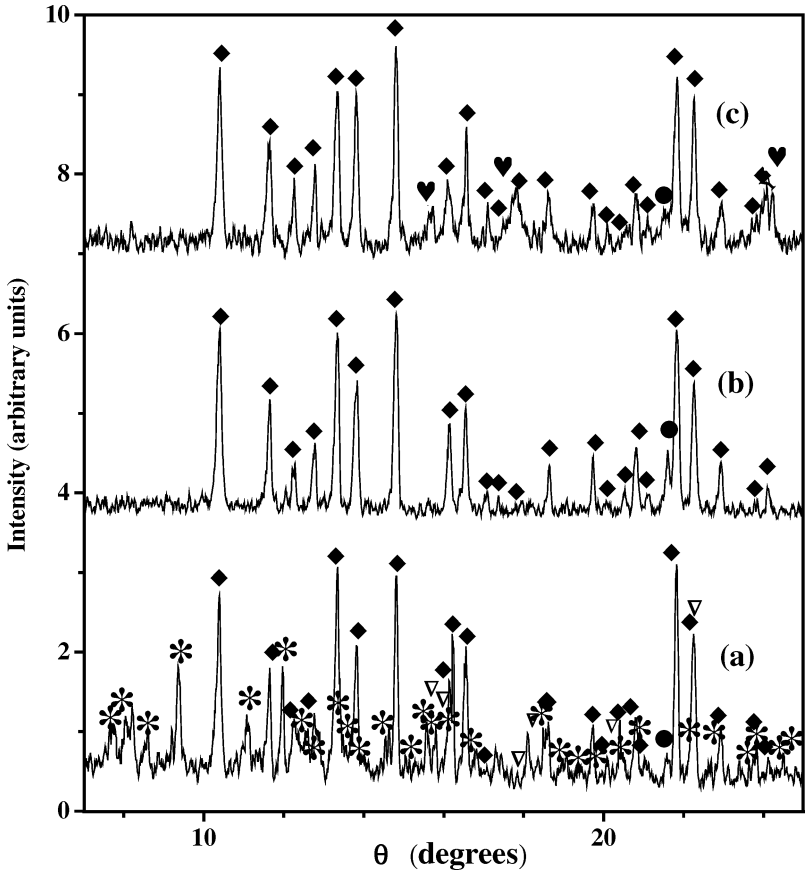

Figure 4 The x-ray diffraction patterns of $CuSO_4 \cdot 5H_2O$-Pb system milled in the planetary mill for (a) 5 min, (b) 30 min and (c) 50 h. ♦ $PbSO_4$, ● Cu, ♥ WC, ∇ Pb, and ∗ $CuSO_4 \cdot 5H_2O$.

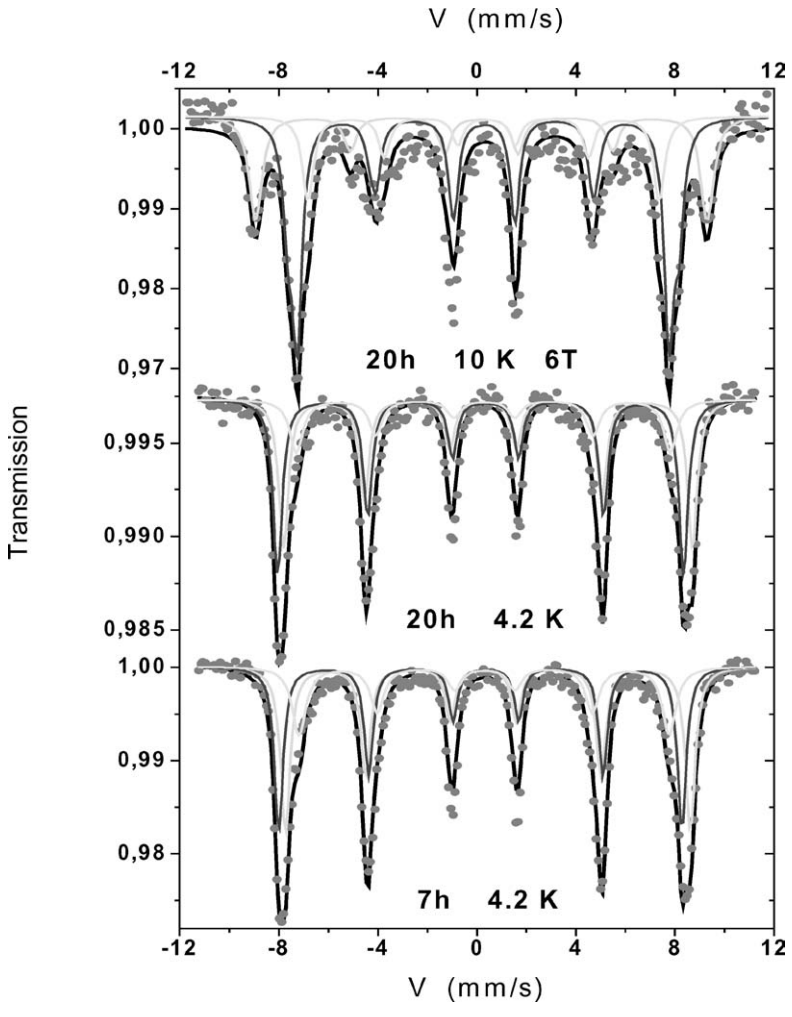

Figure 5 Zero-field Mössbauer spectra recorded at 4.2 K for the 7 h (22 nm) and 20 h (11 nm) milled $ZnFe_2O_4$ samples and the 6 T in-field Mössbauer spectrum recorded at 10 K for the 20 h milled $ZnFe_2O_4$ sample.

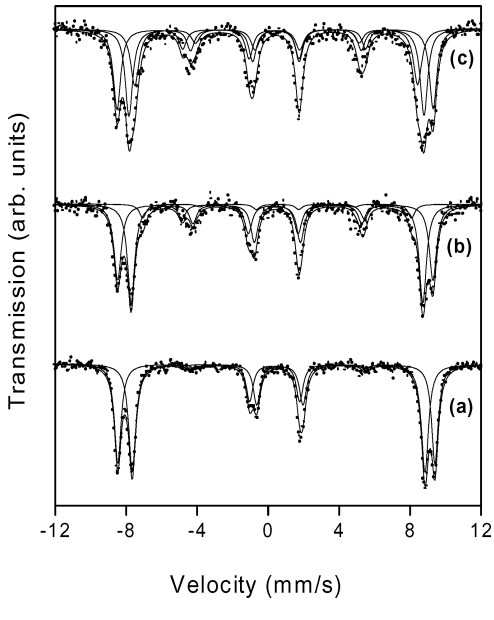

Figure 6 Mössbauer spectra recorded at 4.2 K for the $NiFe_2O_4$ spinel (a) 1-h milled in an external field of 5 T, (b) 20-h milled in an external field of 5 T and (c) 30-h milled in an external magnetic field of 5 T.

at atomic level and can contribute to enhanced reaction kinetics. Thus, not only the driving force, but also factors influencing the diffusion are important in deciding the reaction kinetics in milling. Therefore a careful selection of systems becomes important in the process control.

4. Effect of mechanical energy input on ferrites

The reduction of grain size by mechanical milling has led to interesting results such as changes in cation distributions and spin structure in spinel ferrites [8, 9]. For example, $ZnFe_2O_4$ is an antiferromagnet in its bulk form below 10 K with all the Zn^{2+} ions on A-sites and Fe^{3+} ions on B-sites. When the particle size was reduced to a few nanometers, $ZnFe_2O_4$ exhibited ferrimagnetic ordering even at elevated temperatures

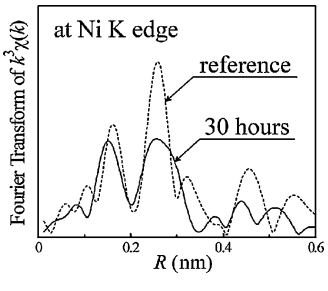

Figure 7 Fourier transformed profiles of bulk nickel ferrite and 30-h milled sample.

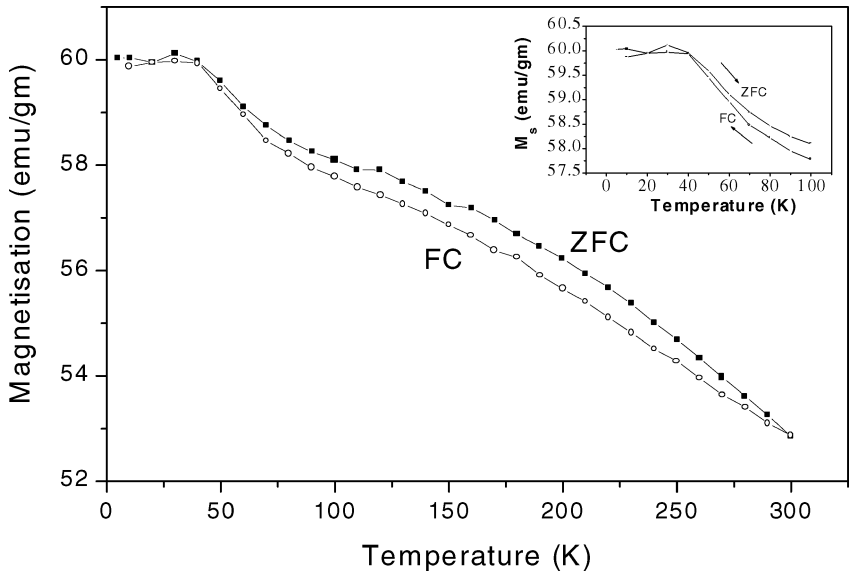

Figure 8 Zero-field-cooled and field-cooled saturation magnetisation curves for the 1-h milled sample in an applied field of 9 T.

[10]. Fig. 5 shows the zero-field Mössbauer spectra recorded at 4.2 K for the 7 h (22 nm) and 20 h (11 nm) milled $ZnFe_2O_4$ samples and the 6 T in-field Mössbauer spectrum recorded at 10 K for the 20 h milled $ZnFe_2O_4$ sample. The splitting of the signals from the A- and B-sites of the spinel in the presence of 6 T magnetic field clearly indicates without any ambiguity that nanocrystalline $ZnFe_2O_4$ is ferrimagnetically ordered.

Similar results have been obtained in the case of $NiFe_2O_4$, which is a well known inverse spinel. In this spinel all the Ni^{2+} ions occupy the octahedral sites and the Fe^{3+} ions are equally distributed between the tetrahedral and octahedral sites. However, when the grain size was reduced to a few nanometer by mechanical milling, we could observe a change in the cation distribution from the inverse spinel to the mixed spinel through our Mössbauer, EXAFS and magnetisation measurements [11]. Fig. 6 shows the Mössbauer spectra recorded at 4.2 K for the $NiFe_2O_4$ spinel (a) 1-h milled (60 nm) in an external field of 5 T, (b) 20-h milled (15 nm) in an external field of 5 T and (c) 30-h milled (10 nm) in an external magnetic field of 5 T. The decrease in the relative intensity of the A-site signal for the sample milled for 30 h compared to that of the 1 h milled sample shows that Fe^{3+} concentration on A-site has decreased due to milling.

The Fourier transformed profiles of the EXAFS spectra, as shown in Fig. 7 describe the sharp peak between 0.2 and 0.3 nm for the bulk reference sample that corresponds to the Ni-Ni or Ni-Fe bond and the peak position suggests that Ni^{2+} ions occupy the octahedral sites. When milled for 30 h this peak is broadened and shifted to farther site. Also, the Ni-O peak at about 0.2 nm has been shifted to a lower distance. The distance between Ni-Ni or Ni-Fe will be 0.292 nm when the Ni ions occupy the octahedral sites alone and hence a sharp peak around 0.292 was observed. On the other hand, when the Ni ions occupy tetrahedral sites alone, the bond length of Ni-Ni or Ni-Fe will be 0.357 nm and a peak will be observed with its maximum around 0.357 nm. If the Ni ions occupy both the sites, we could expect a broad peak containing the peaks due to two different bond lengths. Thus, the corresponding peak would have its maximum at a distance between 0.292 and 0.357 nm. In view of these facts, the profile of the sample milled for 30 nm suggests a partial inversion of Ni ions from octahedral to tetrahedral ions which is reflected in peak broadening and a shift.

The magnetisation of the bulk $NiFe_2O_4$ at 5 K is reported to be 55 emu/g [12] whereas, we have obtained 60 emu/g at the same temperature for the sample with 60 nm grain size. The 8% enhancement in the magnetisation of the latter sample is possible only if some Ni^{2+} ions occupy the tetrahedral sites. These studies therefore demonstrate that there is a change in the cation distribution in nanocrystalline $NiFe_2O_4$ spinel. The ZFC and FC curves (Fig. 8) show that $NiFe_2O_4$ behaves as a spin glass at low temperatures. Fig. 9 shows a variation of Néel temperature with average grain size for the nanocrystalline $NiFe_2O_4$. It is clear that the Néel temperature of the milled samples is higher than that of the bulk sample. The initial increase in the value of Néel temperature on milling is attributed to the change in the cation distribution. The decrease in the Néel

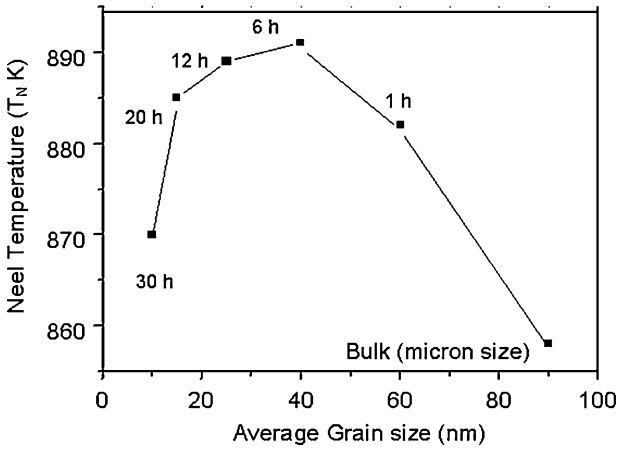

Figure 9 Néel temperature versus average grain size for nanostructured $NiFe_2O_4$. The continuous line is guide to the eye.

temperature after 6 h of milling has been explained on the basis of a combined effect of the change in the cation distribution and finite size effects [13].

5. Concluding remarks

The reactions in the solid state through milling in $CuSO_4 \cdot 5H_2O$-M (M = Mn, Co and Pb) were similar to those in the solution route and were in accordance with the thermodynamic expectation. However the kinetics can deviate from the trend seen in solution. While the barrier of electric double layer decided the kinetics in solution, the diffusivity of metal was found to influence the kinetics in milling of solids. For ferrites the effect is completely different. The change in property flows from the creation of defects, which changes the site occupancy of the species in the ferrite structure leading to different magnetic properties.

References

1. L. TAKACS, *Progr. Mater. Sci.* **46** (2002) 355.
2. P. G. McCORMICK, *Mater. Trans. JIM* **36** (1995) 161.
3. B. S. MURTHY and S. RANGANATHAN, *Internat. Mater. Rev.* **43** (1998) 101.
4. C. SURYANARAYANA, *Progr. Mater. Sci.* **46** (2001) 1.
5. G. B. SCHAFFER and P. G. McCORMICK, *J. Appl. Phy. Lett.* **55** (1989) 45.
6. J. DING, T. TSUZUKI and P. G. McCORMICK, *J. Amer. Ceram. Soc.* **79** (1996) 2956.
7. V. VARGHESE, A. SHARMA and K. CHATTOPADHYAY, *Mater. Sci. Eng.* A **304–306** (2001) 434.
8. S. A. OLIVER, H. H. HAMEH and J. C. HO, *Phys. Rev.* B **60** (1999) 3400.
9. J. Z. JIANG, P. WYNN, S. MORUP, T. OKADA and F. J. BERRY, *Nanostruct. Mater.* **12** (1999) 737.
10. C. N. CHINNASAMY, A. NARAYANASAMY, N. PONPANDIAN, K. CHATTOPADHYAY, H. GUERAULT and J.-M. GRENECHE, *J. Phys.: Condens. Matter.* **12** (2000) 7795.
11. C. N. CHINNASAMY, A. NARAYANASAMY, N. PONPANDIAN, K. CHATTOPADHYAY, K. SHINODA, B. JEYADEVAN, K. TOHJI, K. NAKATSUKA, T. FURUBAYASHI and I. NAKATANI, *Phys. Rev.* B **63** (2001) 184108.
12. J. SMIT and H. P. J. WIJN, "Ferrites" (Phillips Technical Library, Eindhovan, The Netherlands, 1959) p. 157.
13. C. N. CHINNASAMY, A. NARAYANSAMY, N. PONPANDIAN, R. JUSTIN JOSEYPHUS, B. JEYADEVAN, K. TOHJI and K. CHATTOPADHYAY, *J. Magn. Magn. Mater.* **238** (2002) 281.

Received 11 September 2003
and accepted 27 February 2004